J. Earth Planet. Sci. Nagoya Univ., Vol. 45, 17 to 27, 1998

An 85 ± 5 Ma CHIME age for the Agigawa welded tuff sheet in the oldest volcanic sequence of the Nohi Rhyolite, central Japan

Kazuhiro SUZUKI, Mineko NAKAZAKI and Mamoru ADACHI

Department of Earth and Planetary Sciences, Nagoya University, Nagoya 464-8602, Japan
(Received October 24, 1998 / Accepted November 21, 1998)

ABSTRACT

CHIME ages were determined for zircon and allanite from the Agigawa welded tuff sheet of the Nohi Rhyolite in the Kamado area, Gifu Prefecture. The CHIME zircon age is 85 ± 5 Ma and the CHIME allanite age is 86 ± 7 Ma. The Agigawa welded tuff sheet in the lowest volcanic sequence of the Nohi Rhyolite is chronologically identical with the post-tectonic Shinshiro Tonalite (85.2 ± 3.3 – 86.0 ± 4.7 Ma) and the Mitsuhashi Granodiorite (83.8 ± 1.3 – 84.1 ± 3.1 Ma) in the Ryoke metamorphic belt to the south of the Kamado area. Acidic plutonism and volcanism started simultaneously and widely at about 85 Ma after the high T/P Ryoke metamorphism at about 100 Ma.

INTRODUCTION

The Nohi Rhyolite, occupying an area of about 5000 km^2, is the largest cluster of volcanic piles in central Japan. It extends from the northern part of the Ryoke metamorphic belt through the Mino and Circum-Hida terranes to the Hida terrane over a 120 km long in a NW direction; the width is about 40 km. The Nohi Rhyolite consists of numerous welded tuff sheets with lavas and volcaniclastic sediments, and is classified into 6 volcanic sequences defined as the successive accumulation of welded tuff sheets with underlying volcanic sedimentary layers (e.g. Yamada, 1977; Koido, 1991). Rocks of oldest sequence I occur in the southeastern part and those of younger sequences in the central and northwestern parts.

Although the Nohi Rhyolite is inferred to have formed during a long period from late Cretaceous to Paleogene (Koido, 1991) with a climax before 70 Ma (Yamada et al., 1992), the question of when the volcanism had started is left open. The known fact is that rocks of sequence I are intruded by the Inagawa Granodiorite (Sakai et al, 1965; Yamada, 1966). The emplacement age for the Inagawa Granodiorite is still poorly understood, because the pluton had to a great extent undergone thermal effects of successive granite intrusions. Recent CHIME dating, however, discloses that the Inagawa Granodiorite formed at about 82 Ma (Suzuki and Adachi, 1998). A question we address in this paper is whether or not the Nohi Rhyolite volcanism overlapped with the peak Ryoke

metamorphism (100 – 95 Ma, Suzuki et al., 1993, 1994b; Suzuki and Adachi. 1998) and the syntectonic plutonism (95 – 92 Ma, Nakai and Suzuki, 1996; Suzuki and Adachi, 1998). This paper reports CHIME ages of zircon and allanite from a welded tuff sheet in the oldest volcanic sequence of the Nohi Rhyolite in the Kamado area, Gifu Prefecture.

GEOLOGY

The geologic configuration of the Kamado area is given in Fig. 1. The area is underlain mainly by the sedimentary rocks of the Mino terrane, a thick

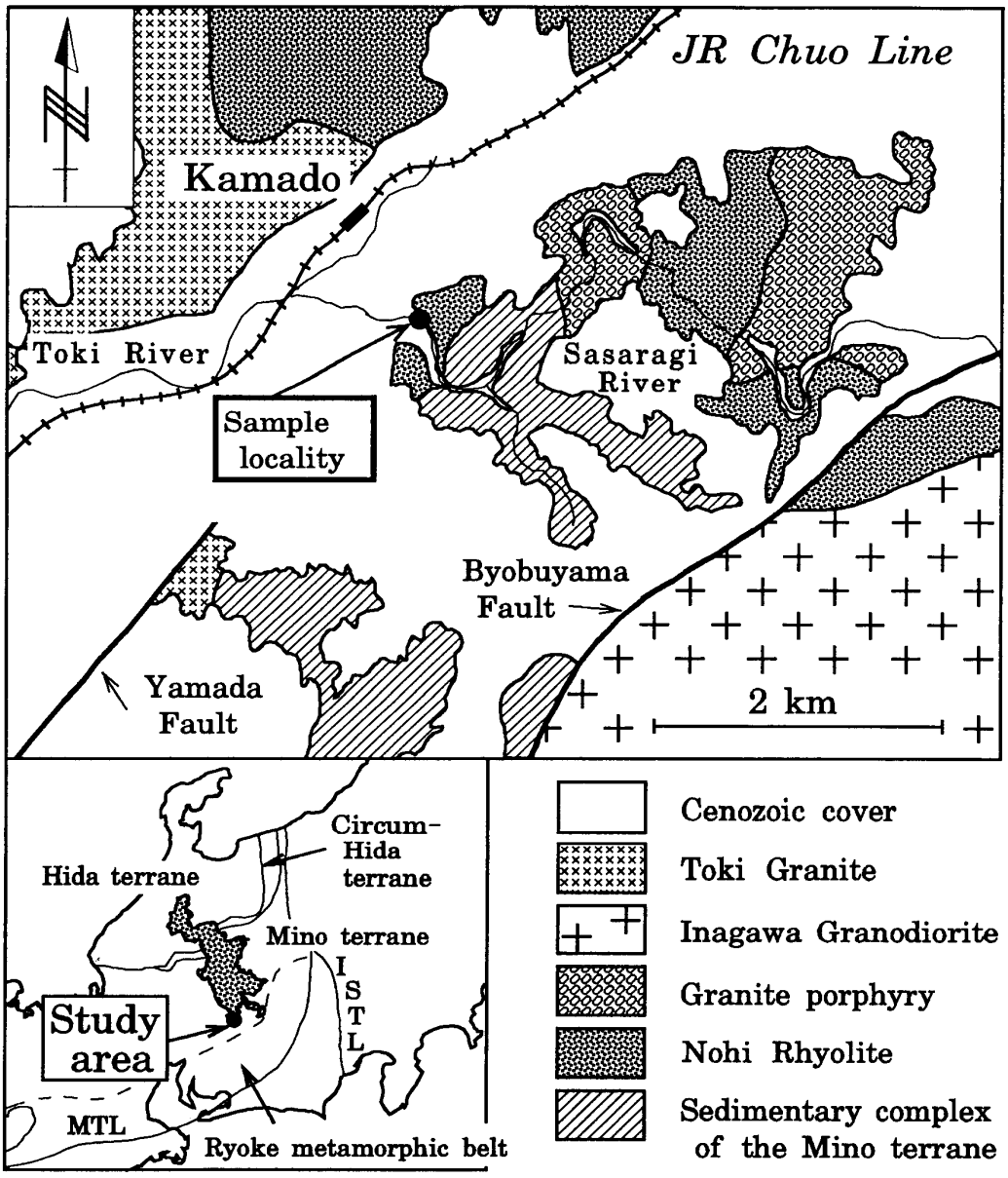

Fig. 1. Geologic map of the Kamado area, Gifu Prefecture, central Japan, showing the sample locality. MTL: the Median Tectonic Line, ISTL: the Itoigawa-Shizuoka Tectonic Line.

welded tuff sheet of the Nohi Rhyolite, granitoids, stocks and dikes of granite porphyry and Cenozoic covers. The sedimentary rocks of the Mino terrane, consisting predominantly of sandstone, shale and chert, underwent extensively thermal metamorphism, and were converted into biotite- and cordierite-hornfels. The welded tuff sheet within the map area, named as the Agigawa welded tuff, is a member of the oldest volcanic sequence of the Nohi Rhyolite (Yamada, 1989). Rocks of this sheet, biotite rhyolite to hornblende-biotite rhyodacite in composition, are densely welded, wholly devitrified and thermally metamorphosed. The Agigawa welded tuff sheet is intruded by small stocks and dikes of granite porphyry. Granitoids in the area are grouped into the Inagawa Granodiorite and the Toki Granite. The Inagawa Granodiorite consists mainly of coarse-grained hornblende-biotite granodiorite and biotite adamellite, and is characterized by the common occurrence of porphyritic K-feldspar. The Toki Granite consists predominantly of medium-grained biotite granite and adamellite.

Sakai et al. (1965) and Yamada (1966) found that the Inagawa Granodiorite had intruded into the Agigawa welded tuff sheet at Kami-giri, Iwamura Town, about 5 km southeast of the map area. The Inagawa Granodiorite, in turn, is intruded by the Toki Granite (Yamada, 1967). Although most granite porphyry stocks are intruded by the Inagawa Granodiorite (Yamada, 1967), granite porphyry dikes in the map area remain immune to thermal metamorphism. We, therefore, presume that granite porphyry dikes, if not all, formed after the emplacement of the Inagawa Granodiorite and Toki Granite.

Previous K-Ar biotite ages show that the emplacement of the Inagawa Granodiorite and the Toki Granite took place at 65 – 70 Ma (Shibata et al., 1962; Kawano and Ueda, 1966). Subsequent Rb-Sr dating by Shibata and Ishihara (1979) reported a 72.3 ± 3.9 Ma whole-rock isochron age as the emplacement time of the Toki Granite. Recent CHIME dating yielded 81.9 ± 1.4 and 82.6 ± 1.8 Ma monazite ages for the Inagawa Granodiorite and a 68.3 ± 1.8 Ma monazite age for the Toki Granite (Suzuki and Adachi, 1998).

SAMPLE DESCRIPTION AND CHIME DATING

The sample (Sample 97121401) for the present CHIME dating was collected from a river-side outcrop of the Sasaragi River (Fig. 1, 32°24'6"N, 137°18'47"E). The rock is dense and porphyritic with a fine-grained matrix of quartz and feldspars (Fig. 2A). Phenocrysts, attaining up to 4 mm in size, make up 40% of the total volume, and are dominated by quartz, plagioclase, K-feldspar and biotite. They are partly corroded. Most biotite phenocrysts are highly distorted and recrystallized along the margin. Rare pumice lenses are completely recrystallized into a fine-grained aggregate of quart and feldspars. Accidental lithic fragments, up to 15 mm in size, constitute only a few volume percent of the rock. They are mainly shale with a subordinate amount of sandstone.

Zircon and allanite occur mainly in close association with distorted biotite phenocrysts, and sometimes as inclusions (Fig. 2B and Fig. 3); they seem to be cogenetic with phenocrystic biotite. Zircon grains range in size from 0.03 to

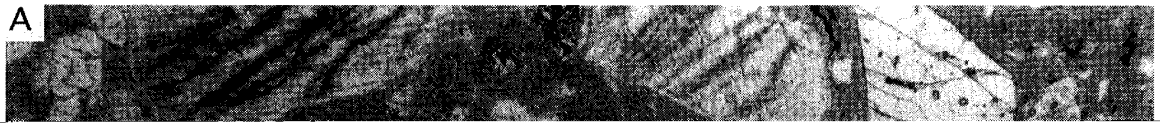
A

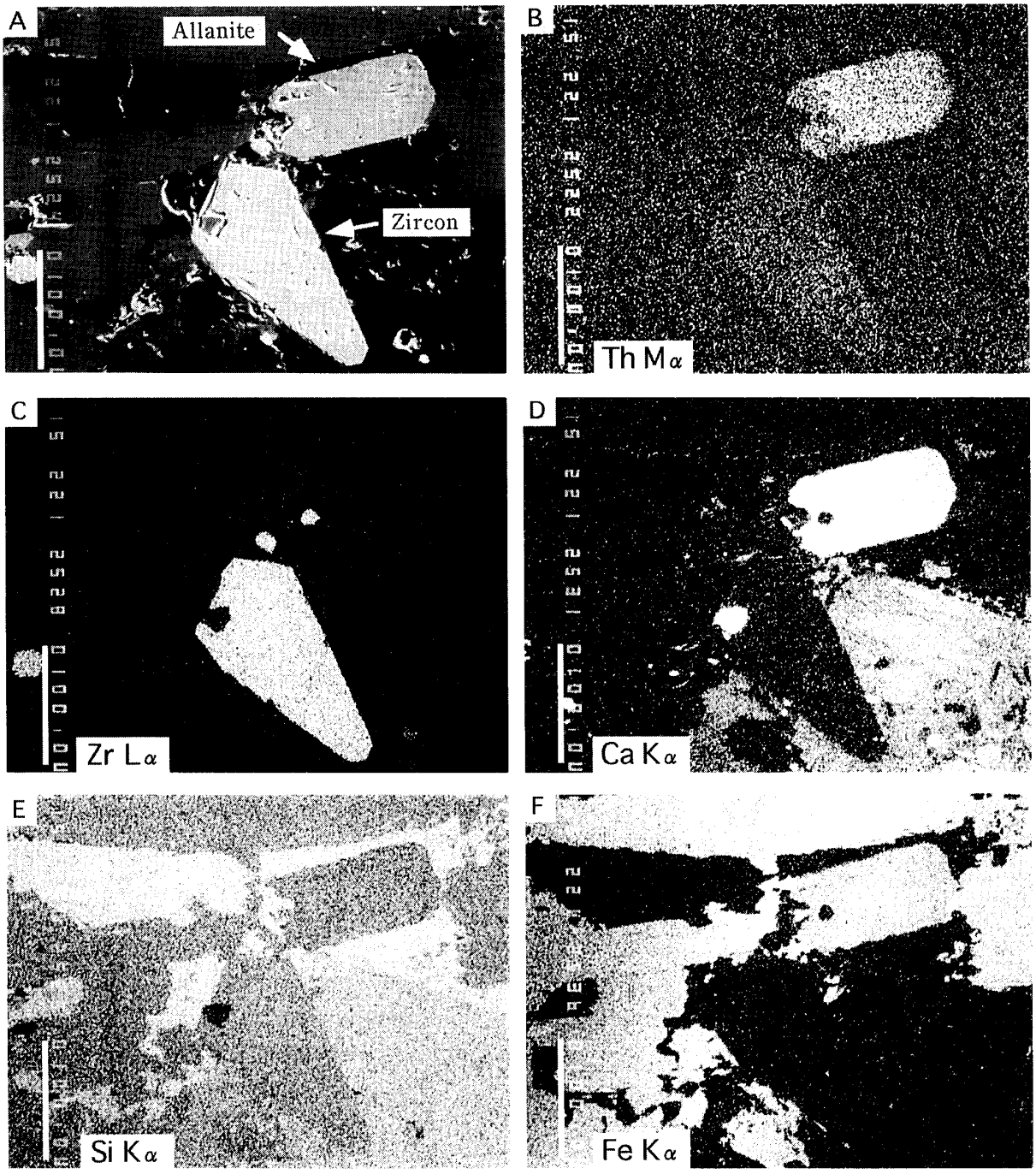

Fig. 3. Backscattered electron and X-ray images of zircon (Z01) and allanite (A04) grains attached on a biotite phenocryst in Sample 97121401. Scale bars are 0.1 mm.

0.18 mm, and show faceted forms of magmatic origin. This morphological character contrasts with the rounded shape of detrital zircon grains in the lithic fragments. Magmatic zircon grains have no visible interior structure under the microscope. Allanite is pleochroic from deep reddish brown to pale brown. Most allanite grains are homogeneous in color, but some show a concentric color zoning with central deep brown and marginal pale brown zones.

Zircon and allanite were analyzed on the JCXA-733 electron microprobe

analyzer equipped with four wavelength dispersive type spectrometers. The instrument operating conditions were 15kV accelerating voltage, 0.35μA probe current and 3μm probe diameter. The ThMα, UMβ, PbMα and YLα only were measured with a PET crystal, and the spectral interference of YLγ on PbMα was corrected through the procedure described by Åmli and Griffin (1975). X-ray intensities were integrated over 400s for the lines and 200s for the backgrounds at two optimum positions on both sides of the lines. The peak and background measurements were repeated twice or three times on zircon, whereas on allanite the damage by electron bombardment prevents repeated measurement. Raw intensity data were converted into concentrations through the method described by Bence and Albee (1968) using analyses of natural zircon (SiO_2 30.5%, ZrO_2 58.8, HfO_2 3.51, Er_2O_3 0.313, Yb_2O_3 0.755% and P_2O_5 1.28%) and allanite (SiO_2 31.6%, Al_2O_3 14.1%, La_2O_3 4.34%, Ce_2O_3 10.1%, Pr_2O_3 0.949%, Nd_2O_3 4.95%, Sm_2O_3 1.01%, Gd_2O_3 0.833%, Dy_2O_3 0.622%, FeO 14.3%, MnO 0.94% and CaO 9.38%) as the matrix compositions. The detection limits of ThO_2, UO_2 and PbO at 2σ confidence level are 0.008%, 0.010% and 0.003% for zircon and 0.009%, 0.012, and 0.004% for allanite, respectively. The relative error in the PbO determination of 0.01 wt.% concentration is about 20% for zircon and 25% for allanite. For the details of the CHIME age calculation, readers are requested to refer Suzuki and Adachi (1991a,b, 1994 and 1998), Adachi and Suzuki (1992) and Suzuki et al. (1994a).

RESULTS

Most zircon grains are low in the Th, U and Pb concentrations, but three grains were found to contain measurable amounts of Pb as well as Th and U. A total of 28 spots on these grains were analyzed, and the analytical results are listed in Table 1 together with apparent ages and UO_2* (the measured UO_2 plus UO_2 equivalent to the measured ThO_2) values. The ThO_2 concentration ranges from 0.073 to 0.898 wt.%, the UO_2 concentration from 0.271 to 1.313 wt.%, and the PbO concentration from 0.0041 to 0.0162 wt.%. The analytical data are plotted linearly on the PbO-UO_2* diagram (Fig. 4A), and give an isochron of 85 ± 5 Ma (MSWD = 0.05) with an intercept value of 0.0002 ± 0.0004.

A total of 80 spots on 7 allanite grains were analyzed, and the results are listed in Table 1 together with apparent ages and ThO_2* (the measured ThO_2 plus ThO_2 equivalents to the measured UO_2) values. Allanite is rich in ThO_2 but poor in UO_2. The ThO_2 concentration ranges from 1.32 to 3.63 wt.%, while the UO_2 concentration varies from 0.013 to 0.122 wt.%. The PbO concentration ranges from 0.0050 to 0.0158 wt.%. All data define a linear array in plot of PbO versus ThO_2* (Fig. 4B), and yields an isochron of 86 ± 7 Ma (MSWD = 0.21) with an intercept value of 0.0010 ± 0.0009.

Table 1. Electron microprobe analyses of ThO_2, UO_2 and PbO of zircons (Z) and allanites (A) in Sample 97121401 from the Agigawa welded tuff sheet of the Nohi Rhyolite in the Kamado area, together with apparent ages, UO_2* (the measured UO_2 plus UO_2 equivalent of the measured ThO_2) and ThO_2* (the measured ThO_2 plus ThO_2 equivalent of the measured UO_2)

Spot No.	ThO2 (wt.%)	UO2 (wt.%)	PbO (wt.%)	Age (Ma)	UO2* (wt.%)
Z01-01	0.205	1.31	0.0161	87	1.38
Z01-02	0.224	0.630	0.0095	101	0.700
Z01-03	0.073	0.319	0.0043	94	0.341
Z01-04	0.185	0.271	0.0042	95	0.329
Z01-05	0.185	0.553	0.0072	88	0.611
Z01-06	0.140	0.327	0.0046	92	0.371
Z01-07	0.135	0.334	0.0041	81	0.376
Z01-08	0.595	0.767	0.0110	86	0.953
Z01-09	0.129	0.338	0.0046	91	0.378
Z01-10	0.372	0.630	0.0091	91	0.746
Z01-11	0.188	0.392	0.0050	83	0.451
Z01-12	0.537	0.771	0.0108	86	0.939
Z01-13	0.220	0.374	0.0051	86	0.443
Z01-14	0.464	0.583	0.0079	81	0.728
Z01-15	0.832	0.905	0.0134	86	1.17
Z01-16	0.110	0.305	0.0041	90	0.339
Z01-17	0.112	0.371	0.0049	90	0.406
Z01-18	0.128	0.365	0.0044	81	0.405
Z01-19	0.177	0.361	0.0048	86	0.416
Z02-01	0.183	0.445	0.0063	93	0.502
Z02-02	0.145	0.464	0.0062	91	0.509
Z02-03	0.125	0.451	0.0062	94	0.490
Z02-04	0.109	0.393	0.0049	85	0.427
Z03-01	0.133	0.314	0.0047	98	0.355
Z03-02	0.668	0.479	0.0075	81	0.687
Z03-03	0.467	0.410	0.0065	87	0.556
Z03-04	0.485	0.417	0.0058	76	0.568
Z03-05	0.898	0.564	0.0097	86	0.844

Spot No.	ThO2 (wt.%)	UO2 (wt.%)	PbO (wt.%)	Age (Ma)	ThO2* (wt.%)
A01-01	3.31	0.049	0.0133	91	3.47
A01-02	1.76	0.020	0.0060	78	1.82
A01-03	1.53	0.026	0.0064	94	1.61
A01-04	1.81	0.026	0.0094	117	1.89
A01-05	2.81	0.045	0.0121	97	2.95
A01-06	2.51	0.042	0.0109	98	2.64
A01-07	2.20	0.034	0.0088	90	2.31
A01-08	2.43	0.042	0.0113	104	2.56
A01-09	2.26	0.038	0.0104	103	2.38
A01-10	1.84	0.043	0.0083	99	1.97
A01-11	2.23	0.031	0.0089	90	2.33
A01-12	2.14	0.046	0.0087	90	2.28
A02-01	3.03	0.085	0.0137	98	3.30
A02-02	2.60	0.078	0.0106	88	2.85
A02-03	2.98	0.081	0.0125	91	3.24
A02-04	2.97	0.089	0.0132	96	3.26
A02-05	2.80	0.077	0.0127	99	3.04
A02-06	2.67	0.073	0.0117	95	2.90
A02-07	2.64	0.076	0.0118	97	2.88
A02-08	2.66	0.081	0.0123	100	2.92
A02-09	2.61	0.072	0.0104	87	2.83
A02-10	2.62	0.082	0.0122	100	2.88
A02-11	3.63	0.092	0.0158	95	3.93
A02-12	2.91	0.079	0.0118	88	3.16
A02-13	2.85	0.094	0.0123	92	3.15
A02-14	1.32	0.013	0.0060	104	1.36
A03-01	3.53	0.067	0.0145	91	3.75
A03-02	2.83	0.064	0.0128	100	3.03
A03-03	3.42	0.086	0.0139	89	3.70
A03-04	2.51	0.052	0.0102	90	2.68
A03-05	2.48	0.061	0.0107	95	2.67
A03-06	2.46	0.056	0.0106	95	2.64
A03-07	3.58	0.084	0.0141	86	3.86
A03-08	3.24	0.076	0.0134	91	3.48
A04-01	2.43	0.068	0.0104	93	2.65
A04-02	2.74	0.087	0.0105	82	3.02
A04-03	2.88	0.080	0.0118	89	3.13
A04-04	2.69	0.076	0.0121	98	2.93
A04-05	2.70	0.076	0.0133	107	2.95
A04-06	2.77	0.081	0.0119	93	3.03
A04-07	3.40	0.100	0.0141	90	3.72
A04-08	3.13	0.098	0.0142	97	3.45
A04-09	2.80	0.091	0.0116	89	3.10
A04-10	2.91	0.082	0.0142	106	3.17
A05-01	2.02	0.036	0.0091	101	2.14
A05-02	1.75	0.035	0.0089	113	1.86
A05-03	1.97	0.035	0.0081	92	2.08
A05-04	1.97	0.044	0.0106	119	2.11
A05-05	1.59	0.019	0.0069	99	1.65
A05-06	1.63	0.019	0.0077	108	1.69
A05-07	1.63	0.018	0.0050	70	1.68
A05-08	2.06	0.042	0.0084	91	2.19
A05-09	2.32	0.060	0.0099	93	2.52
A05-10	2.34	0.062	0.0101	94	2.54
A05-11	2.37	0.067	0.0100	91	2.58
A05-12	2.58	0.069	0.0128	108	2.80
A05-13	2.38	0.050	0.0091	85	2.54
A05-14	2.27	0.054	0.0098	95	2.44
A05-15	2.05	0.037	0.0108	118	2.17
A05-16	1.47	0.017	0.0066	102	1.53
A05-17	1.55	0.024	0.0055	80	1.63
A05-18	2.10	0.048	0.0089	93	2.25
A05-19	1.81	0.029	0.0080	100	1.90
A06-01	3.10	0.078	0.0118	83	3.35
A06-02	2.90	0.074	0.0110	83	3.14
A06-03	3.61	0.090	0.0158	96	3.90
A06-04	3.58	0.122	0.0152	91	3.97
A06-05	3.37	0.091	0.0143	92	3.67
A06-06	2.21	0.053	0.0109	108	2.38
A06-07	3.22	0.081	0.0133	90	3.48
A07-01	2.66	0.034	0.0104	89	2.77
A07-02	3.30	0.062	0.0139	94	3.50
A07-03	2.81	0.053	0.0110	87	2.98
A07-04	3.58	0.057	0.0149	94	3.76
A07-05	2.48	0.042	0.0126	114	2.62
A07-06	3.11	0.051	0.0132	95	3.27
A07-07	2.85	0.040	0.0109	87	2.98
A07-08	2.82	0.037	0.0107	86	2.94
A07-09	2.76	0.043	0.0099	81	2.90
A07-10	2.98	0.044	0.0118	89	3.12

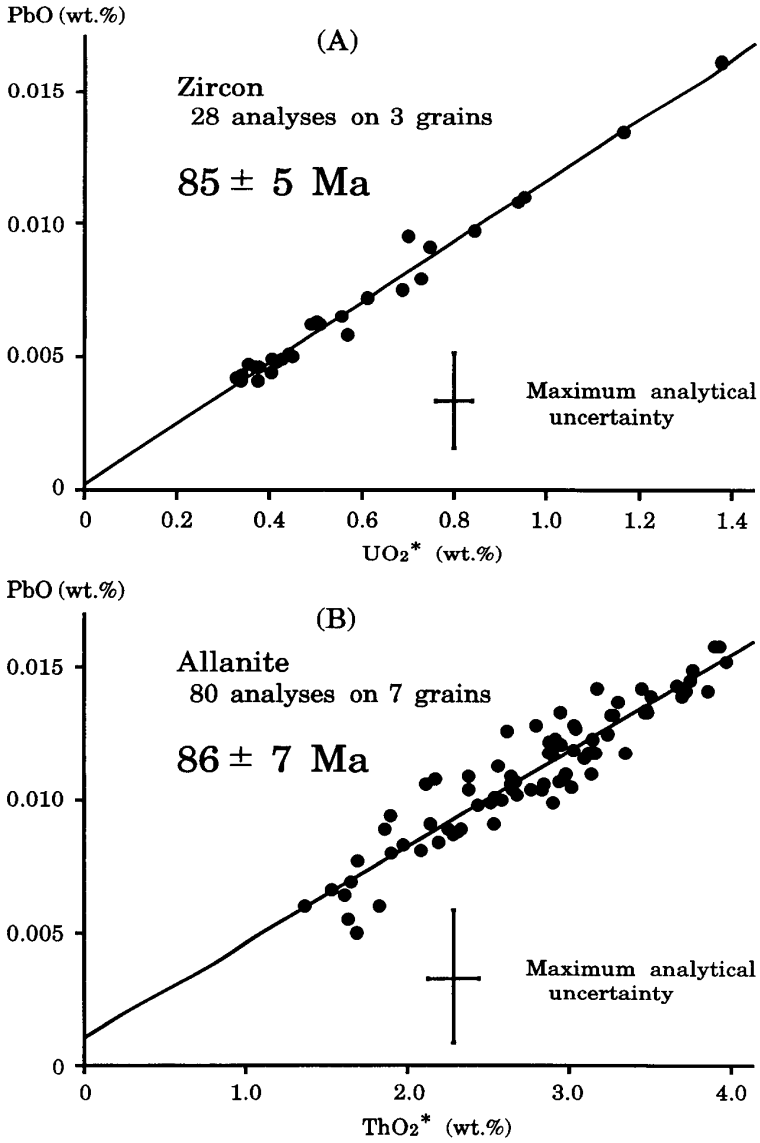

Fig. 4. Plots of PbO vs. UO_2* of 28 analytical data on 3 zircon grains (A) and PbO vs. ThO_2* of 80 analytical data on 7 allanite grains (B) in Sample 97121401. Error bars in the figures represent 2σ analytical uncertainty, and error given to the age is of 2σ.

DISCUSSION AND CONCLUDING REMARKS

The CHIME zircon and allanite ages for the the Agigawa welded tuff sheet in the oldest volcanic sequence of the Nohi Rhyolite are 85 ± 5 and 86 ± 7 Ma, respectively. The ages coincide well with each other within the limit of analytical uncertainty, and are likely to show the eruption time of the Agigawa welded tuff. As mentioned earlier, the Agigawa welded tuff sheet is intruded by the Inagawa Granodiorite (Sakai et al., 1965; Yamada, 1966). Since the CHIME monazite ages of the Inagawa Granodiorite are 81.9 ± 1.4 and 82.6 ± 1.8 Ma (Suzuki and Adachi, 1998), the ca. 85 Ma CHIME ages for the Agigawa welded tuff sheet are in agreement with the geologic relation.

The present CHIME zircon and allanite ages are placed in the context of the

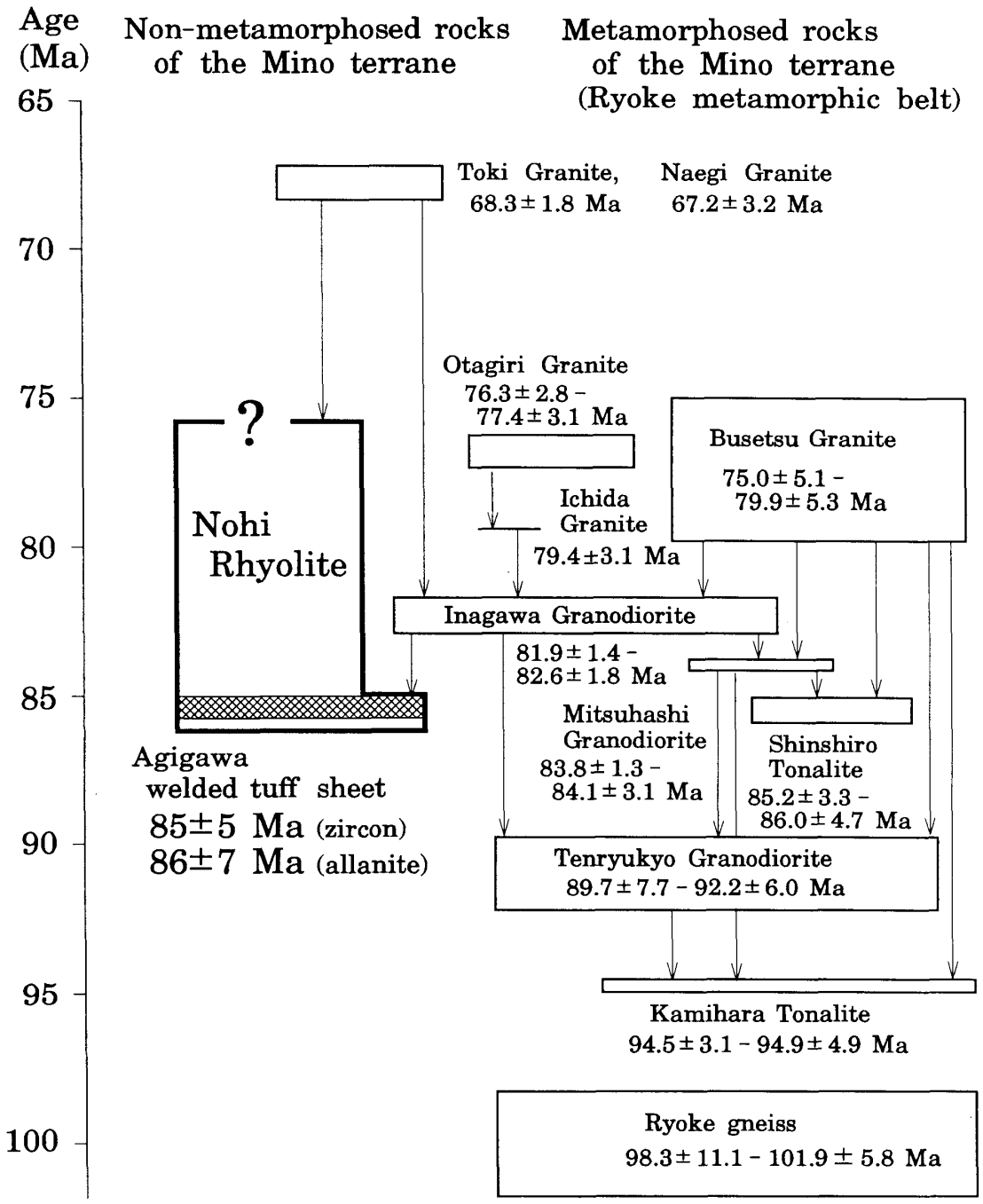

Fig. 5. Comparison of CHIME zircon and allanite ages for the Agigawa welded tuff sheet in the oldest volcanic sequence of the Nohi Rhyolite with CHIME monazite ages for granitoids and gneisses in the Ryoke metamorphic belt.

intrusive relation of granitoids in the Ryoke metamorphic belt (Fig. 5), together with the previously reported CHIME ages for gneisses and granitoids (Suzuki et al., 1994a,b, 1995; Morishita and Suzuki, 1995; Nakai and Suzuki, 1996; Suzuki and Adachi, 1998). The CHIME zircon and allanite ages of the Agigawa welded tuff sheet are distinctly younger than the monazite ages for the Ryoke gneiss (98.3 ± 11.1 – 101.9 ± 5.8 Ma, Suzuki et al., 1994a,b), but are nearly identical

with the CHIME monazite ages for the Shinshiro Tonalite (85.2 ± 3.3 – 86.0 ± 4.7 Ma, Morishita and Suzuki, 1995) and the Mitsuhashi Granodiorite (83.8 ± 1.3 – 84.1 ± 3.1 Ma, Suzuki et al., 1994a,b). These granitoids, occurring in higher grade parts of the Ryoke metamorphic belt, have been regarded as the Older Ryoke Granites (Ryoke Research Group, 1972). The Shinshiro tonalite, however, is known to have intruded discordantly into the Ryoke gneiss, and overprinted the andalusite-orthoclase assemblage on the regional assemblage of sillimanite-orthoclase (Asami and Hishino, 1980: Miyake et al., 1992). The Shinshiro Tonalite and the subsequent Mitsuhashi Granodiorite are of shallow emplacement than the Tenryukyo Granodiorite with a contact assemblage of sillimanite-orthoclase, and appear to have been controlled by tectonics different from those for the Tenryukyo Granodiorite and the syntectonic Kamihara Tonalite. Although we are uncertain whether the Agigawa welded tuff sheet has a petrogenetic relation with the Shinshiro Tonalite and the Mitsuhashi Granodiorite or not, we can state that post-tectonic acidic magmatism started simultaneously at about 85 Ma in both non-metamorphosed and metamorphosed parts of the Mino terrane.

ACKNOWLEDGEMENTS

We would like to express our thanks to Dr. N. Yamada for a particularly careful review, and to Mr. S. Yogo for his technical assistance. This work was supported in part by Grant-in-Aid for fundamental Scientific Research (Nos. 09304048 and 09640568) from the Ministry of Education, Science and Culture, Japan.

REFERENCES

Adachi, M. and Suzuki, K. (1992) A preliminary note on the age of detrital monazites and zircons from sandstones in the Upper Triassic Nabae Group, Maizuru terrane. *Mem. Geol. Soc. Japan*, No.38, 111–120.

Åmli, R. and Griffin, W.L. (1975) Microprobe analysis of REE minerals using empirical correction factors. *Am. Mineralogist*, **60**, 599–606.

Asami, M. and Hoshino, M. (1980) Staurolite-bearing schists from the Hongu-san area in the Ryoke metamorphic belt, central Japan. *Jour. Geol. Soc. Japan*, **86**, 581–591.

Bence, A.E. and Albee, A.L. (1968) Empirical correction factors for the electron microanalysis of silicates and oxides. *J. Geol.*, **76**, 382–403.

Kawano, Y. and Ueda, Y. (1966) K-A dating on the igneous rocks in Japan (V) – Granitic rocks in southwestern Japan –. *Jour. Min. Pet. Econ. Geol.*, **56**, 191–211.

Koido, Y. (1991) A Late Cretaceous-Paleogene cauldron cluster: the Nohi Rhyolite, central Japan. *Bull. Volcanol.*, **53**, 132–146.

Miyake, A., Murata, E. and Morishita, O. (1992) Growth stages of andalusite in the Ryoke metamorphic rocks from the Nukata area, Aichi Prefecture. *Jour. Min. Pet. Econ. Geol.*, **87**, 475–480.

Morishita, T. and Suzuki, K. (1995) CHIME ages of monazite from the Shinshiro Tonalite of the Ryoke belt in the Mikawa area, Aichi Prefecture. *J. Earth Planet. Sci., Nagoya Univ.*, **42**, 45–53.

Nakai, Y. and Suzuki, K. (1996) CHIME monazite ages of the Kamihara Tonalite and the Tenryukyo Granodiorite in the eastern Ryoke belt of central Japan. *Jour. Geol. Soc. Japan*, **102**, 431–439.

Ryoke Research Group; Hayama, Y., Ikeda, K., Jindo, O., Kagami, H., Kijima, T., Kutsukake, T., Morimoto, M., Nakai, Y., Nakasuji, A., Sekido, S., Suzuki, K., Yamada, N., and Yamada, T. (1992) The mutual relations of the granitic rocks of the Ryoke metamorphic belt in central Japan. *Earth Science (Chikyu Kagaku)*, **26**, 205–216.

Sakai, E., Otani, M., Sugioka, K., Hayakawa, M., Mizutani, T., Noda, I., Miyoshi, K., Miura, H., Matsuoka, S., Hattori, Y. and Ito, R. (1965) Preliminary note on the order of intrusion of the Mesozoic igneous rocks in the three cities of Mizunami, Ena and Nakatsugawa and in the Ena district, Gifu Prefecture, central Japan. *Bull. Aichi Gakugei Univ., Natural Science*, **14**, 61–71.

Shibata, K. and Ishihara, S. (1979) Rb-Sr whole-rock and K-Ar mineral ages of granitic rocks in Japan. *Geochem. J.*, **13**, 113–119.

Shibata, K., Miller, J.A., Yamada, N., Kawada,K. Murayama, M. and Katada, M. (1962) Potassium-argon ages of the Inagawa Granite and Naegi Granite. *Bull. Geol. Surv. Japan*, **13**, 317–320.

Suzuki, K. and Adachi, M. (1991a) Precambrian provenance and Silurian metamorphism of the Tsubonosawa paragneiss in the South Kitakami terrane, Northeast Japan, revealed by the chemical Th-U-total Pb isochron ages of monazite, zircon and xenotime. *Geochem. J.*, **25**, 357–376.

Suzuki, K. and Adachi, M. (1991b) The chemical Th-U-total Pb isochron ages of zircon and monazite from the Gray Granite of the Hida Terrane, Japan. *J. Earth Sci., Nagoya Univ.*, **38**, 11–37.

Suzuki, K. and Adachi, M. (1994) Middle Precambrian detrital monazite and zircon from the Hida gneiss on Oki-Dogo Island, Japan: their origin and implications for the correlation of basement gneiss of Southwest Japan and Korea. *Tectonophysics*, **235**, 277–292.

Suzuki, K. and Adachi, M. (1998) Denudation history of the high T/P Ryoke metamorphic belt, southwest Japan: constraints from CHIME monazite ages of gneisses and granitoids. *J. Metamorphic. Geol.*, **16**, 23–37.

Suzuki, K., Adachi, M. and Kajizuka, I. (1994a) Electron microprobe observations of Pb diffusion in metamorphosed detrital monazites. *Earth Planet. Sci. Lett.*, **128**, 391–405.

Suzuki, K., Morishita, T., Kajizuka, I., Nakai, Y., Adachi, M. and Shibata, K. (1994b) CHIME ages of monazites from the Ryoke metamorphic rocks and some granitoids in the Mikawa-Tono area, central Japan. *Bull. Nagoya Univ. Furukawa Museum*, No.10, 17–38.

Suzuki, K., Nasu, T. and Shibata, K. (1995) CHIME monazite ages of the Otagiri and Ichida Granites in the Komagane area, Nagano Prefecture. *J. Earth Planet. Sci., Nagoya Univ.*, **42**, 17–30.

Yamada, N. (1966) Presence of Ryoke Granite intruding into the Nohi Rhyolite and its geologic significance. *Jour. Geol. Soc. Japan*, **72**, 355–358.

Yamada, N. (1967) Nohi Rhyolite and granitoids in the area to the south of Ena-city. in: N. Yamada, K. Kawada, Y. Nakai and H. Isomi (eds) Granitoids and Nohi Rhyolite in the Tono district. *Guidebook for excursion 6 of 1967 Ann. Meeting Geol. Soc. Japan*, pp18–27.

Yamada, N. (1977) Nohi Rhyolite and associated granitic rocks. in: N. Yamada, T. Nozawa and Y. Hayama (eds) Mesozoic felsicigneous activity and related metamorphism in central Japan – from Nagoya to Toyama. *Guidebook for excursion 4. Geol. Surv. Japan*, pp33–60.

Yamada, N. (1989) Late Cretaceous Ena Cauldron found in the southernmost part of the Nohi Rhyolitic Mass, central Japan. *Monograph Assoc. Geol. Colloab. Jpn.*, No.36, 21–34.

Yamada, N., Shibata, K., Tsukuda, E., Uchiumi, S., Matsumoto, T., Takagi, H. and Akahane, H. (1992) Radiometric ages of igneous rocks around the Atera Fault, central Japan, with special reference to the age of activity of the Atera Fault. *Bull. Geol. Surv. Japan*, **43**, 759–779.